LARGE-SCALE RESPONSE OF THE CALIFORNIA CURRENT TO FORCING BY THE WIND STRESS CURL

DUDLEY B. CHELTON
Jet Propulsion Laboratory
California Institute of Technology
Pasadena, California 91109

ABSTRACT

Seasonal distributions of zooplankton volume in the California Current show a maximum at a distance of about 100 km offshore between San Francisco and northern Baja California. It is shown that this coincides with a region of offshore upwelling of the thermocline associated with a nearshore counterflow. This counterflow is evident year-round at depths below the thermocline (the California Undercurrent) but appears only seasonally in the upper 200 m (the Davidson Countercurrent). However, the integrated nearshore transport in the upper 500 m is poleward year-round.

The seasonal California Current-Countercurrent system is shown to have a nonseasonal (anomalous) counterpart that fluctuates with a time scale of 5-6 months. The region of offshore upwelling associated with this anomalous pattern is found to be located somewhat farther (about 200-300 km) offshore than in the seasonal pattern. Statistical analysis of this anomalous pattern of variability reveals a response resembling that expected from a simple model of offshore Ekman pumping (upwelling) driven by the wind stress curl. As such, this upwelling is not a boundary phenomenon and is therefore quite distinct from coastal upwelling in this region.

It is proposed that this Ekman pumping mechanism upwells nutrients into the euphotic zone, and is therefore indirectly responsible for the offshore peak in zooplankton abundance north of the northern Baja California border.

RESUMEN

Las distribuciones estacionales del volumen del zooplancton en la Corriente de California señalan un máximo a unos 100 Km. mar afuera, entre San Francisco y la zona norte de Baja California. Se demuestra que ésto coincide con la región de surgencia de la termoclina, asociada con una contracorriente costera. Este flujo costero se manifiesta todo el año a profundidades por debajo de la termoclina (contracorriente de California), pero es de régimen estacional por encima de los 200 m de profundidad (contracorriente Davidson). Sin embargo, integrando el transporte costero de componente norte que abarca de los 500 a los 0 m de profundidad, puede considerarse que dicho flujo dura todo el año.

Se demuestra que el sistema estacional, Corriente de California-Contracorriente, tiene una anomalía que no es estacional, y que fluctúa en periodos de 5-6 meses. La región de surgencias asociada con estas anomalías, se encuentra localizada más lejos, hacia los 200-300 Km. mar afuera del patrón estacional. El análisis estadístico de la variabilidad en este tipo de anomalía revela una respuesta similar a la que pudiera resultar de un simple modelo de Ekman, bombeo en las surgencias, desarrollado por la acción de los remolinos del viento. En este caso la surgencia no es producida por la acción de zonas limítrofes, siendo por lo tanto distinta a las surgencias costeras que se presentan en esta región.

Se considera que este mecanismo de bombeo Ekman aporta nutrientes a la zona eufótica, y es responsable indirectamente de los máximos en la abundancia de zooplancton al norte de Baja California.

INTRODUCTION

Through the persistent efforts of CalCOFI over the past 30 years, sufficient data has now accumulated to allow statistical examination of physical and biological interaction in the California Current over a broad range of time and space scales. Past investigations by Bernal (1979; 1981), Bernal and McGowan (1981), Chelton (1981), and Chelton, Bernal, and McGowan (in press) have focused on the very large spatial scales of variability. These studies have demonstrated that zooplankton biomass and the transport of the California Current are dominated by variability with time scales of 2 years and longer. A rather surprising discovery from these studies has been that these interannual variations appear to be unrelated to local wind forcing over the California Current.[1] This study represents an attempt to isolate some (secondary) aspect of the flow of the California Current that *is* driven

[Manuscript received February 15, 1982.]

[1] An apparent weak relation between the flow of the California Current and basin-wide scales of wind forcing over the North Pacific has been shown by Chelton, Bernal, and McGowan (in press) to actually reflect a coupling between the California Current and occurrences of El Niño in the eastern tropical Pacific. This results from the fact that large-scale winds over the North Pacific are significantly correlated with El Niño events.

by the local wind forcing in this region and to compare it with dynamical expectations.

The conventional view of the dynamics of epipelagic ecosystems in eastern boundary currents is that biological productivity at all levels of the food chain is indirectly controlled by wind-driven coastal upwelling of deep-water nutrients (see, for example, Smith 1968; Cushing 1969; 1975; Walsh 1977). Winds over the California Current are generally upwelling-favorable year-round south of San Francisco. Although this is undoubtedly an important factor contributing to the high nutrient concentrations found in the California Current (and thus the high levels of productivity), it is not necessarily the only controlling factor. Advection of nutrient-rich waters from higher latitudes by the equatorward transport of the California Current may also be important. The fact that the dominant large-scale variations in zooplankton abundance are unrelated to variations in wind forcing indicates that coastal upwelling must play at best a secondary role in the biological variability. The earlier studies by Bernal, Chelton, and McGowan have presented rather convincing evidence that advection is the dominant mechanism controlling large-scale, year-to-year variations in zooplankton abundance.

Although the dominant signals of variability in the California Current are unrelated to the local wind field, it seems reasonable to expect that some secondary aspect of variability in the physical characteristics must be related to wind forcing. If such a relationship could be identified, the results might have important biological implications.

ZOOPLANKTON DISTRIBUTION IN THE CALIFORNIA CURRENT

A limitation of the earlier studies by Bernal, Chelton, and McGowan has been that the large spatial averaging used to isolate the larger scales of variability precludes the possibility of detecting any cross-shore structure in either zooplankton biomass or current velocity. For example, if coastal upwelling were solely responsible for productivity, we might expect zooplankton abundance to be maximum at the coast, decreasing offshore. This relationship between nearshore and offshore zooplankton biomass would be obscured in the large areal averaging of zooplankton volume. However, the spring-summer distribution of zooplankton volume shown in Figure 1 indicates that this anticipated nearshore-offshore structure is present only south of CalCOFI line 100. Between San Francisco and northern Baja California the highest zooplankton biomass is located a distance of about 100 km from the coast. It is worth noting that satellite images of this region from the Coastal Zone Color Scanner (CZCS) frequently indicate extremely high chlorophyll concentrations immediately adjacent to the coast (within 10-20 km), presumably reflecting a phytoplankton response to nutrients from coastal upwelling (see, for example, Smith and Baker 1982). Thus, it is possible that an even larger peak in zooplankton biomass may exist very close to the coast, but this narrow region is not well sampled by the standard CalCOFI station pattern. Even if concentrations are higher near shore, the offshore peak in zooplankton abundance is an important biological characteristic of the California Current.

There are at least two possible explanations for this feature. The first is that nutrients upwelled at the coast by the longshore wind stress lead to high phytoplankton productivity within a relatively short time lag (the doubling time for phytoplankton is less than a few days). This high primary productivity would then result in a corresponding increase in secondary productivity. The zooplankton responding to the increased phytoplankton biomass would be passively carried offshore together with nonconsumed phytoplankton by Ekman transport from the longshore wind stress. However, since the doubling times for zooplankton are on the order of a month, the zooplankton biomass could actually increase offshore, even though the primary food source is at the coast. Eventually, as the zooplankton continued to drift offshore, food would become a limiting factor, and zooplankton biomass would decrease. Given an appropriate primary-secondary productivity model, this mechanism could, in principle, be quantitatively tested from the 30-year CalCOFI data set. However, the spatial and temporal sampling of both phytoplankton and zooplankton in the CalCOFI record are probably inadequate for this type of study.

An alternative explanation is that the region offshore is, for reasons yet to be determined, a more hospitable environment for the zooplankton and that the high zooplankton biomass is produced locally rather than being passively carried into the region by Ekman drift. Because the time scales are longer, this mechanism can easily be investigated from the CalCOFI data.

THE NEARSHORE COUNTERFLOW OF THE CALIFORNIA CURRENT

The July longshore integrated transport in the upper 500 m in the California Current is shown in Figure 2. (Most of this transport is generally confined to the upper 200 m.) Note that the peak in zooplankton abundance north of CalCOFI line 100 coincides with a region of maximum horizontal shear in the flow. The nearshore transport is poleward while the transport

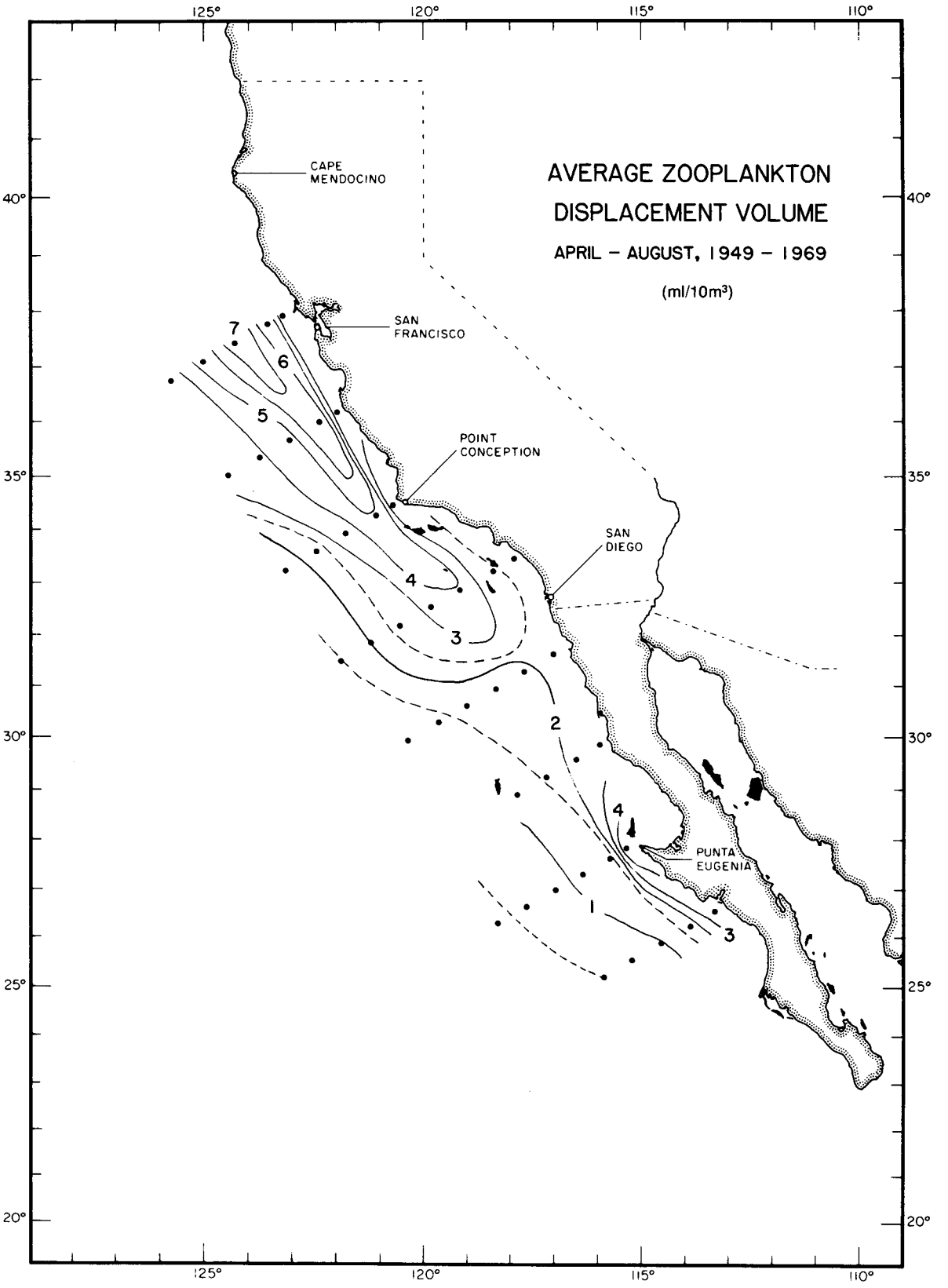

Figure 1. Spring-summer distribution of zooplankton displacement volume in the California Current. April-August long-term (1949-69) averages were computed over "pooled areas" measuring 200 km in the longshore direction and 65 km in the cross-shore direction (see Smith 1971). The dots represent the centers of the pooled areas. This spatial and temporal averaging removes the small-scale patchiness inherent in the zooplankton samples.

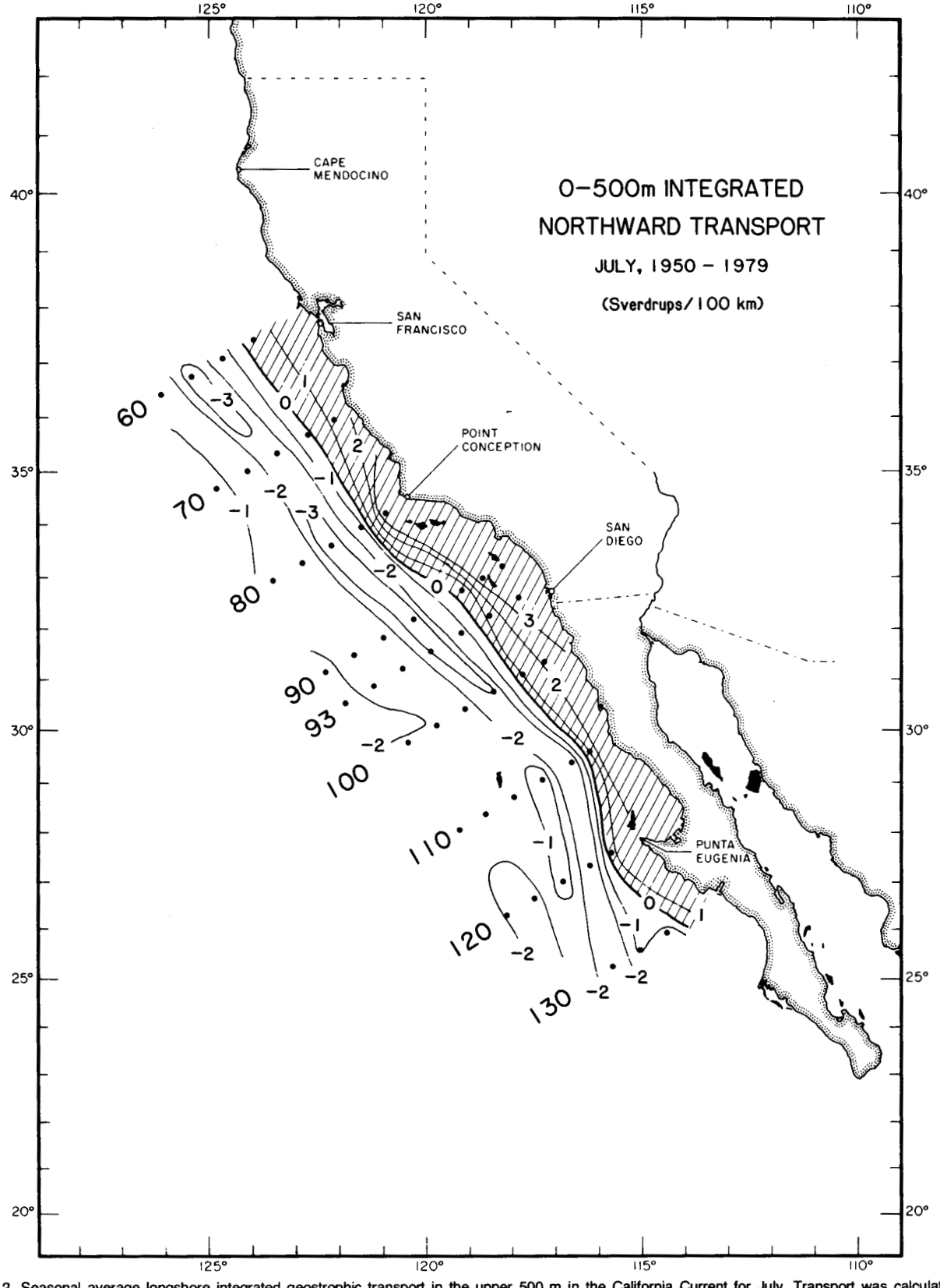

Figure 2. Seasonal average longshore integrated geostrophic transport in the upper 500 m in the California Current for July. Transport was calculated from geostrophic velocities relative to a reference level of 500 db (dots show location of stations used to draw contours, and the CalCOFI line numbers are labeled). Shaded region represents poleward transport. These seasonal mean values were determined by the harmonic method, which fits the full 30-year time series at each grid location to two harmonics (one with an annual and the other a semiannual period) by least squares regression.

farther offshore is equatorward. The flow in the region of maximum zooplankton biomass is very weak. This "recirculation" area would thus provide a very stable environment with little tendency to disperse the zooplankton populations.

The relation between zooplankton biomass and the transport of the California Current is shown in detail in Figure 3 for each of the CalCOFI cardinal lines from 60 to 120. For lines 60 through 90, the peaks in zooplankton volume are all located approximately 50-150 km offshore. In all cases, this very nearly coincides with the location of flow reversal as determined from the integrated transport in the upper 500 m. (The zooplankton maximum is located somewhat inshore of the flow reversal along line 70, but this may be attributable to the different methods used to compute the seasonal means; namely, long-term averaging for zooplankton and harmonic analysis for geostrophic transport.) For lines 100 through 120, the zooplankton biomass is maximum immediately adjacent to the coast, even though there is still a region of flow reversal 50-100 km offshore. Zooplankton productivity is apparently controlled by a different physical process in this southern region (perhaps coastal upwelling as opposed to the offshore upwelling that will be discussed for the northern area).

It should be emphasized at the outset that the analysis described here restricts attention to the physical characteristics of the California Current. Speculations about the possible biological response expected to be associated with the observed physical variability will be discussed. The validity of the proposed biological-physical connection could be easily tested from the 30-year CalCOFI record of zooplankton biomass.

The nearshore counterflow is a prevalent feature of the California Current system. The seasonal mean steric heights of the sea surface relative to 500 db for the months of January, April, July, and October are shown in Figure 4. Since gradients of steric height are proportional to the strength of the geostrophic flow, the steric height contours can be used to infer relative velocity. The nearshore surface counterflow is always present inside the Southern California Bight and present everywhere north of central Baja California during the fall and winter. (When it appears north of Point Conception, the nearshore counterflow is generally called the Davidson Countercurrent.) This feature exists year-round as a relatively steady "undercurrent" in the deeper water throughout the California Current as shown by the seasonal mean steric heights of the 200-db surface relative to 500 db in Figure 5.

Thus, the flow of the California Current can be characterized as a superposition of two "modes" of variability. One consists of a nearshore poleward counterflow extending from the surface down to at least 500 m and an equatorward flow from the surface to at least 500 m in the region offshore. This first

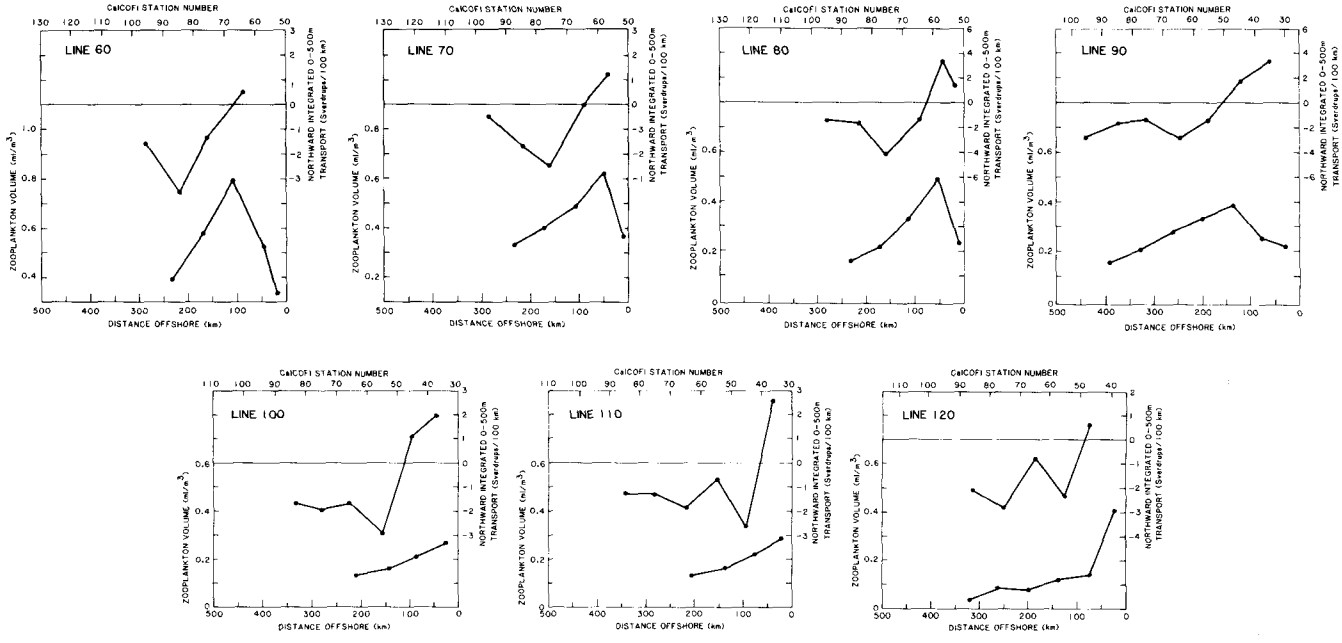

Figure 3. Cross sections of 0-500 m July seasonal average longshore integrated geostrophic transport (upper curves) and April-August average zooplankton displacement volumes (lower curves) for each of the CalCOFI cardinal lines from 60 to 120 (see Figure 2 for locations). Zooplankton averages were computed over 120-km-by-65-km pooled areas (see Smith 1971).

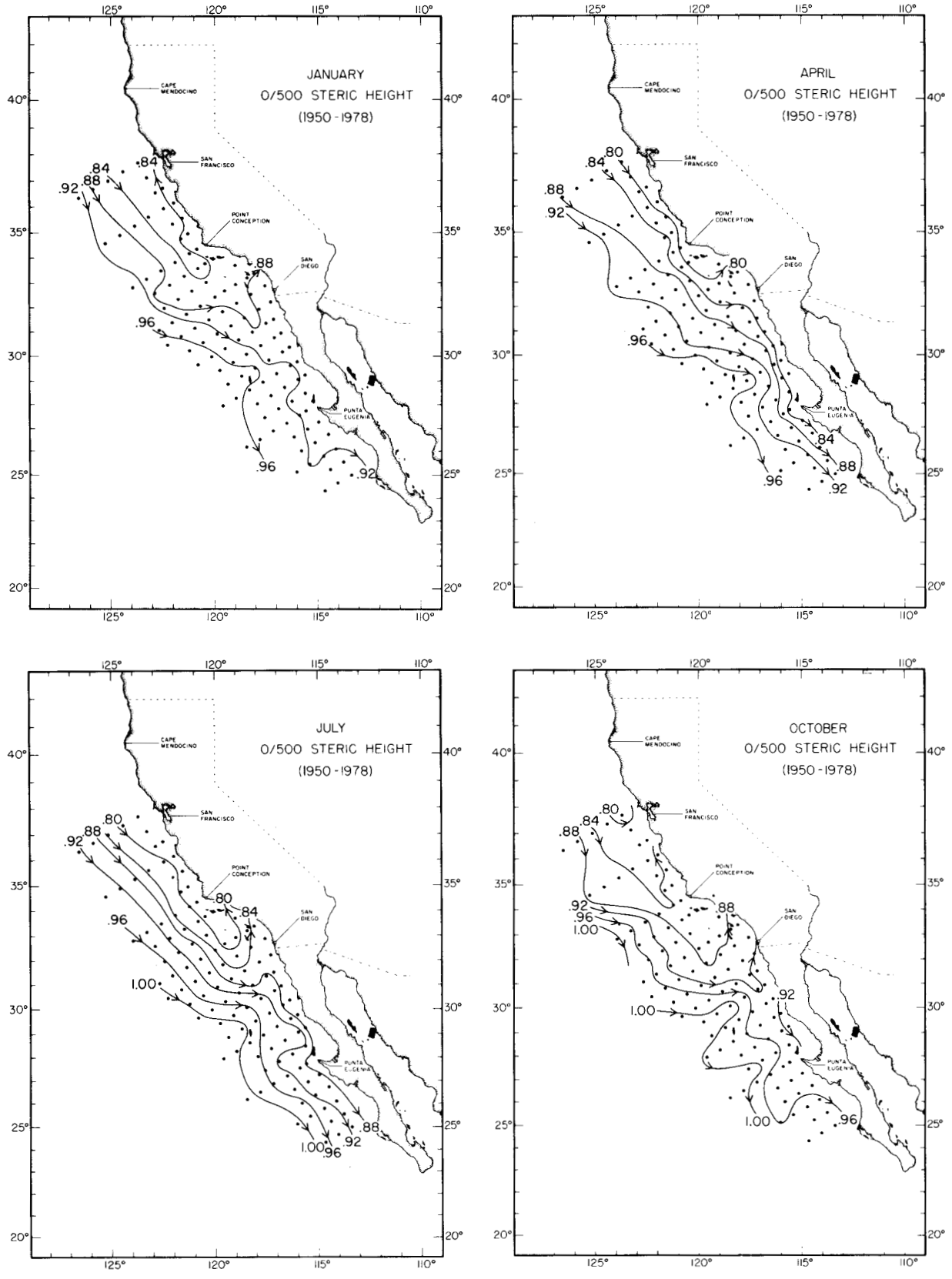

Figure 4. January, April, July, and October seasonal mean values of the steric height of the sea surface relative to 500 db. Arrows on contours indicate direction of geostrophic flow (computed from gradients of the steric height). Averages were computed over the 30-year period from 1950-80 using harmonic analysis as described in Figure 2.

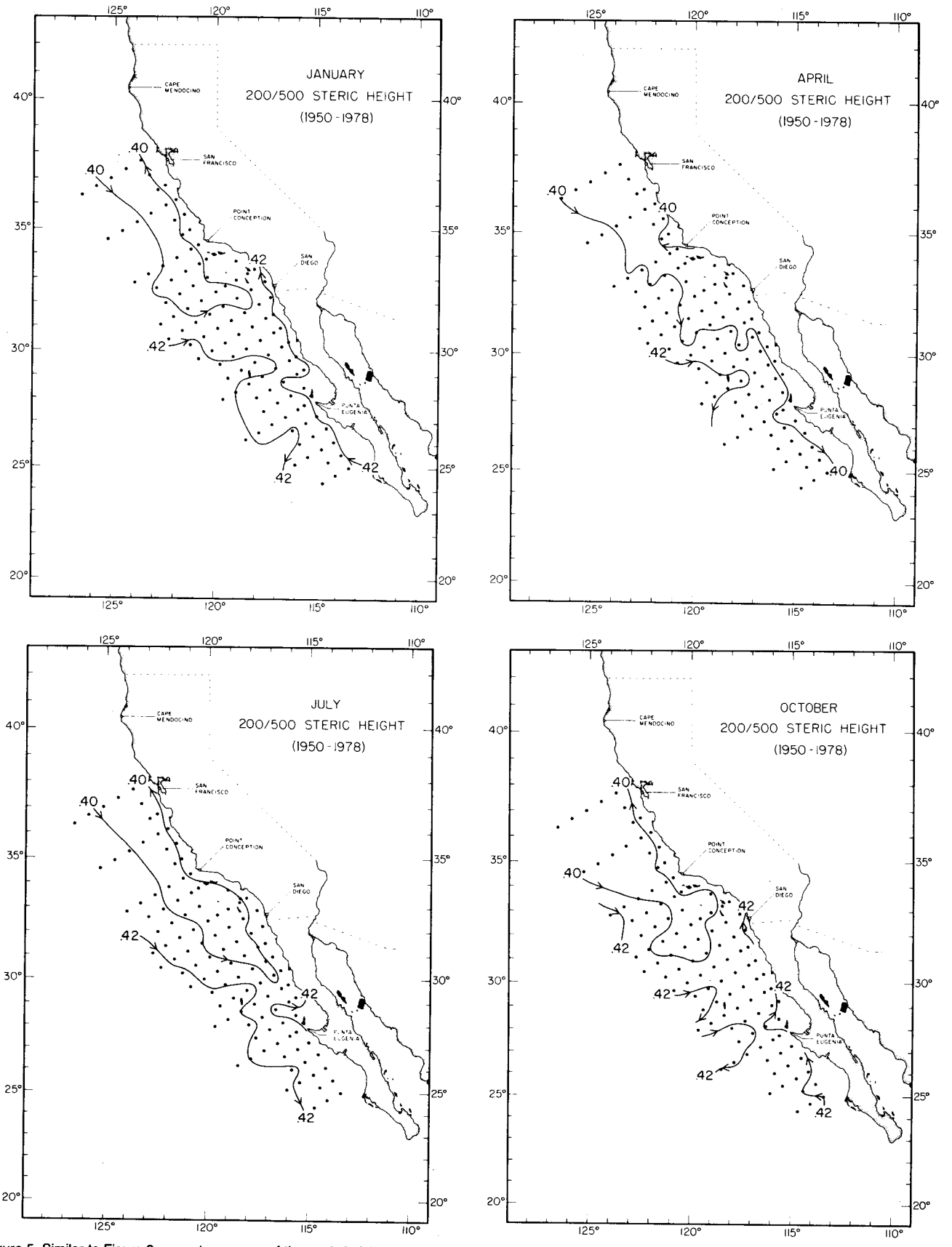

Figure 5. Similar to Figure 3, except maps are of the steric height at 200 db relative to 500 db.

mode varies only weakly over the seasonal cycle. The second mode consists of a shallow equatorward near-surface flow everywhere, with strong seasonal variability. When this second mode is weak (late fall and early winter) the nearshore counterflow associated with the first mode is evident everywhere from the surface to 500 m. However, when the second mode is strong (late spring and early summer) the nearshore counterflow associated with the first mode is reduced (or disappears altogether) near the surface. At these times the counterflow is evident only as a deep undercurrent.

A look at what a nearshore-offshore surface flow reversal means in terms of thermocline depth discloses a second important biological implication of this feature. A schematic diagram for a simple two-layer system is shown in Figure 6. For a nearshore surface poleward geostrophic flow, the sea surface must slope downward *away* from the coast. Correspondingly, an equatorward surface geostrophic flow in the region offshore requires a sea-surface slope downward *toward* the coast. The sea-surface height is minimum in the middle region where the flow is weak. If the flow in the deeper layer is zero or weak relative to the near-surface flow, then the offshore trough in sea level must be compensated by an offshore doming of the thermocline. Thus, in this simplified two-layer model, the region of flow reversal corresponds to a region of maximum vertical displacement (upwelling) of deep-water isotherms (and hence, nutrients). The deep-water nutrients supplied to the surface layer by this mechanism would result in high primary productivity, which would then lead to the observed high zooplankton abundance in this region (Figure 1).

Sections of temperature across the California Current verify the thermocline behavior suggested from the simple two-layer model (Figure 7). The upward doming of deep-water isotherms offshore is present year-round (with some seasonal variation) throughout the California Current. It should be emphasized that the upwelling discussed here is *not* directly a coastal boundary phenomenon. Coastal upwelling from the longshore wind stress is only a nearshore process restricted to within 20-50 km of the coast (Yoshida 1955; Allen 1973; Gill and Clarke 1974). This coastal-boundary-related upwelling is evident in Figure 7 as rising isotherms at the nearest inshore stations. The upwelling region emphasized in this study is located about 100-150 km offshore.

The section of nutrient concentrations along line 90 shown in Figure 8 indicates that this offshore upwelling is indeed an important source of nutrients to the euphotic zone (evident by the upward doming of nutrient contours about 100-200 km offshore). Measurements of nutrients are inadequate to construct long-term average distributions throughout the California Current. However, the 0-50-m integrated nitrate shown in Figure 9 indicates that the offshore nutrient enrichment was present everywhere north of northern Baja California during August-September 1969.

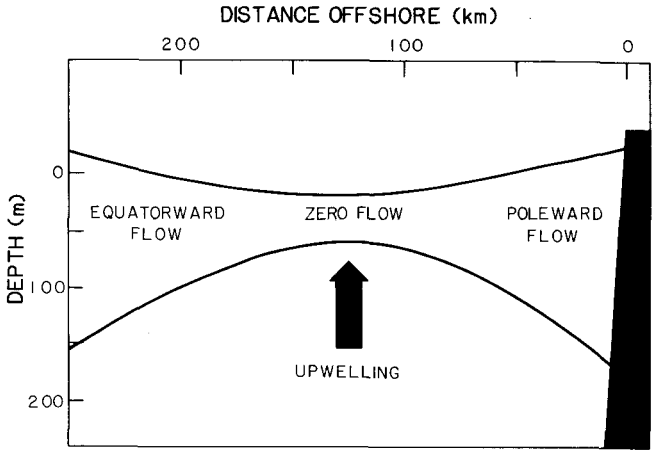

Figure 6. Schematic diagram of two-layer system showing the sea-surface and thermocline configuration corresponding to an equatorward flow offshore and a nearshore poleward flow.

Satellite chlorophyll images provide additional evidence for the existence of an offshore enrichment of nutrients. In addition to the coastally trapped high chlorophyll concentrations discussed previously, the CZCS images often show regions of high chlorophyll concentrations approximately 100-150 km offshore (see, for example, Smith and Baker 1982). These features are commonly referred to as "plumes," since they sometimes appear to extend offshore from Point Conception or other points farther north. This term is somewhat misleading because it implies that the high phytoplankton biomass is due to nutrients advected downstream from a source at the coast. Since these plumes of chlorophyll often extend several hundred kilometers, the supply of nutrients at a single upstream coastal source would have to be enormous. It seems more likely that the entire plume is a continuous source of nutrients brought to the sea surface by non-coastal upwelling.

A SEARCH FOR THE CAUSE OF THE NEARSHORE COUNTERFLOW

In the preceding section it was suggested that the offshore peak in zooplankton abundance in Figure 1 may be related to the upwelling of deep-water isotherms and nutrients associated with a nearshore counterflow. But what is the cause of this counterflow? It cannot be driven by the longshore wind stress itself because the prevailing winds over the

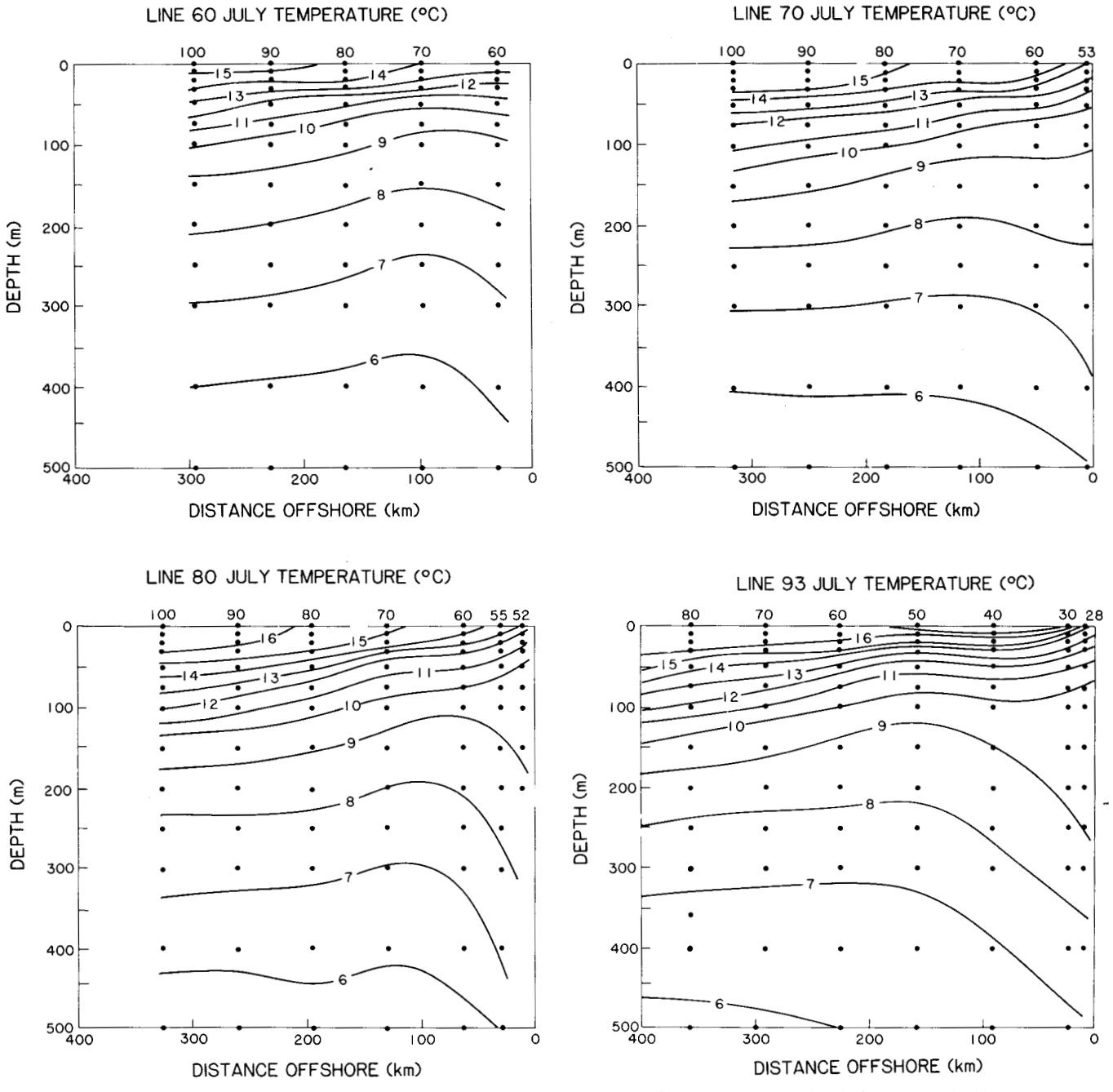

Figure 7. Average July temperature sections along CalCOFI lines 60, 70, 80, and 93 (see Figure 2 for locations) computed by the harmonic method (see text) over the 30-year period 1950-79. CalCOFI station numbers are shown along the top of each plot.

California Current are equatorward year-round south of San Francisco. So the counterflow, when it is present, is in opposition to the overlying winds.

It has long been recognized that the generally equatorward longshore winds over the California Current reach their maximum speed some distance offshore. This "jet" of winds results in a change in sign of the wind stress curl: inshore of the jet, the wind stress curl is positive, while farther offshore it is negative (as it is over most of the interior Pacific Ocean). These features are clearly evident in the seasonal mean wind stress curl maps shown in Nelson (1977) and Chelton (1980). The spatial resolution of existing historical data is too coarse to resolve the detailed characteristics of the wind field in this region. However, it appears that the boundary where the wind stress curl changes sign is roughly parallel to the coast and located somewhere between 200 and 400 km

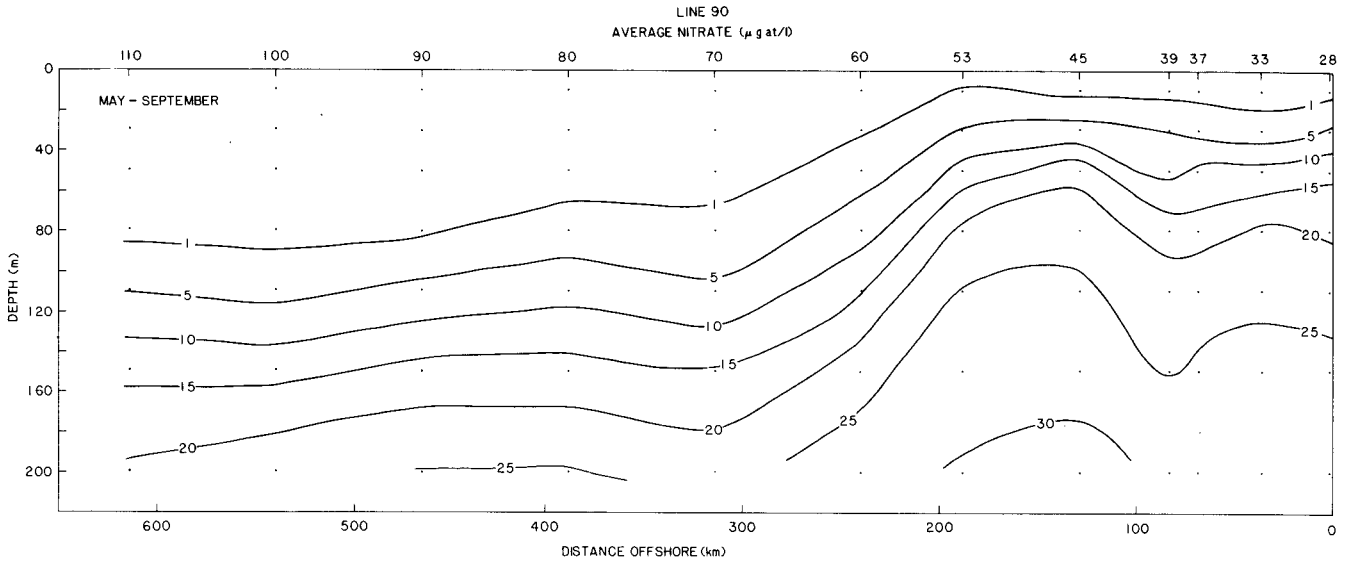

Figure 8. Spring-summer vertical distribution of nitrate along CalCOFI line 90. Data taken from 1969, 1972, and 1978.

offshore. The curl magnitude deduced from these coarse-resolution winds is largest immediately adjacent to the coast.

This nearshore positive wind stress curl makes the dynamics of the California Current system very interesting. If we denote the northward water velocity by v, the depth by z, the characteristic water density by ρ, the vector wind stress by $\vec{\tau}$ (with northward and eastward components τ_y and τ_x), and the Coriolis parameter by $f = 2\Omega\sin\theta$ (where Ω is the earth's rotation rate and the θ is the latitude), Sverdrup (1947) showed that the steady-state response to the wind stress curl is given by

$$\int_{-\infty}^{-o} v\,dz = \frac{1}{\rho\beta}\,\text{curl}\,\vec{\tau} = \frac{1}{\rho\beta}\left(\frac{\partial\tau_y}{\partial x} - \frac{\partial\tau_x}{\partial y}\right).$$

Thus, because of the latitudinal variation of the Coriolis parameter $\beta = \frac{df}{dy}$, a positive wind stress curl leads to a poleward vertically integrated "Sverdrup transport." In the California Current, the nearshore positive wind stress curl would lead to a nearshore poleward water transport in opposition to the prevailing equatorward winds.

Munk (1950) used observations of winds over the California Current to show that the general character of the counterflow observed from hydrographic observations was consistent with the Sverdrup relation. This is also shown qualitatively in Figure 10 with more recent data. The upper panel shows the nearshore integrated transport in the upper 500 m at 36° N, 122° W. Except for April and May, when there is no net transport, the integrated transport is poleward all year with a maximum in November. This poleward transport appears to lag the wind stress curl (middle panel) by about 3-4 months and is in opposition to the consistently equatorward wind stress (lower panel).[2]

Yoshida and Mao (1957) later reexamined the wind-forced response of the California Current in somewhat greater detail. They pointed out that classical coastal upwelling is restricted to within a very narrow region close to the coast and that large-scale upwelling in the California Current must be driven by the wind stress curl. They also noted that the readjustment of the ocean to seasonally changing wind stress curl forcing cannot occur instantly. (This may account for the 3-4-month lag between wind stress curl and maximum poleward transport evident in Figure 10.) Thus, the thermocline depth is related to the integral effect of the wind stress curl, or, equivalently, the time rate of change of the thermocline depth (upwelling) is related to the instantaneous wind stress curl. This dynamical balance is now referred to as "Ekman pumping" (c.f., Pedlosky 1979) and can be expressed in terms of the sea-surface elevation h by:

$$\frac{dh}{dt} = -\frac{1}{\rho f}\,\text{curl}\,\vec{\tau}.$$

[2]The wind stress and wind stress curl data used in this study were computed from quasi-geostrophic wind vector estimates by Fleet Numerical Oceanography Center (FNOC). The FNOC grid spacing is about 300 km at the latitudes examined in this study. A detailed description of the method used by FNOC to compute the wind stress and wind stress curl can be found in Caton et al. (1978). Values were computed at 6-hourly intervals and then averaged to form monthly means. These are the best measure of wind stress and wind stress curl presently available for examining variability over the time scales of interest in this study.

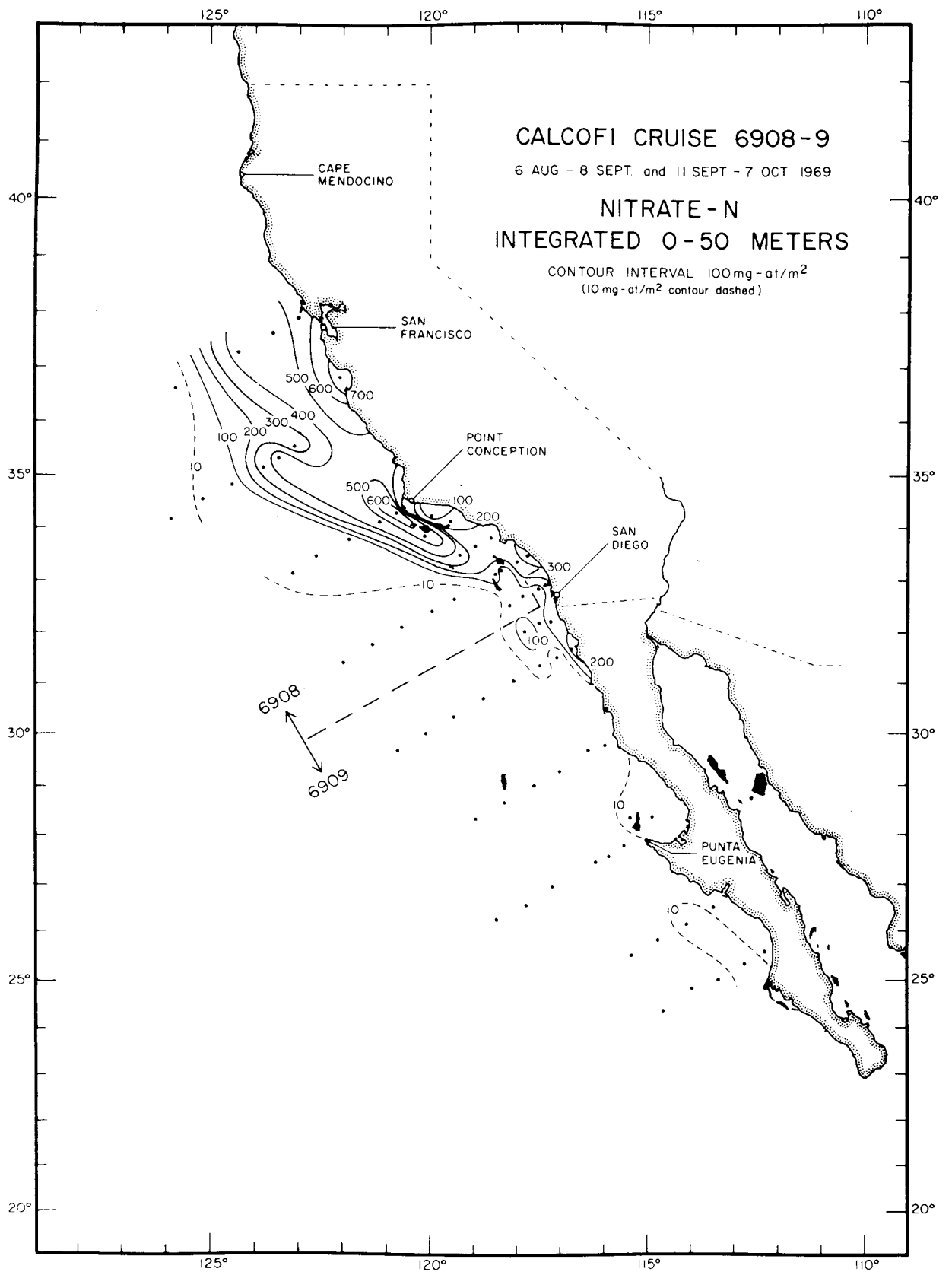

Figure 9. Horizontal distribution of 0-50-m integrated nitrate for CalCOFI cruises from August 6 to October 7, 1969 (from Thomas and Siebert 1974).

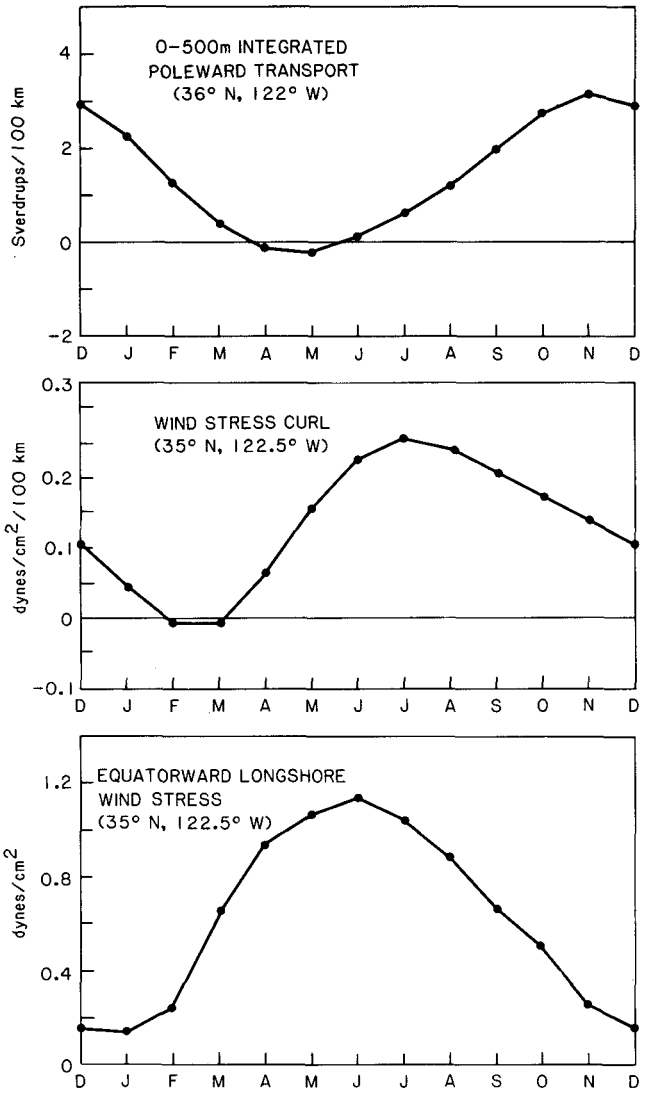

Figure 10. *Upper panel:* seasonal variation of the longshore integrated geostrophic transport in the upper 500 m (computed from geostrophic velocities relative to 500 db) between stations 55 and 60 along CalCOFI line 70 (located at 36°N, 122°W). Positive values correspond to poleward flow. *Middle panel:* seasonal variation of the wind stress curl at 35°N, 122.5°W. *Lower panel:* seasonal variation of equatorward longshore wind stress at 35°N, 122.5°W. Wind stress curl and wind stress data consist of FNOC quasi-geostrophic winds on a grid with approximately 600 km resolution (see text). These seasonal cycles were computed by the harmonic method discussed in Figure 2.

Thus, a positive wind stress curl causes a downward vertical velocity of the sea surface. This drop in sea level corresponds to a *rise* of the thermocline, i.e., a positive wind stress curl causes upward vertical velocity (upwelling) of the thermocline and a corresponding upwelling of deep-water nutrients.

It should be noted that, when the latitudinal variation of the Coriolis parameter is taken into account, the transient response to wind stress curl described by (2) generates westward-propagating Rossby waves, which ultimately bring the ocean into the steady-state Sverdrup balance (1). Since the phase speeds of Rossby waves are small (less than 10 cm/sec), the transient adjustment to changing wind stress curl would require a time scale of at least 2-3 months to bring the California Current into steady-state equilibrium.

STATISTICAL RELATIONSHIPS

The relationship between the wind stress curl and the countercurrent suggested qualitatively above cannot be examined quantitatively from the seasonal cycles. The reason for this is that nearly all geophysical quantities show a strong seasonal variation, and any two seasonal cycles are likely to be highly correlated if one allows for a phase lag. However, the statistical reliability of any resulting high correlation is very low. Chelton (in press) gives examples of how this can lead to erroneous conclusions about cause and effect.

Briefly, the presence of any narrow band signal (annual cycle, semiannual cycle, tidal cycle, etc.) reduces the effective number of degrees of freedom or independent realizations in a time series. A purely random, white-noise time series with N sample observations contains N degrees of freedom. At the other extreme, a pure-tone harmonic time series contains only 2 degrees of freedom, no matter how long the record length is or how frequently the harmonic signal is sampled. Since seasonal variability generally consists of two harmonics, one with an annual and the other with a semiannual period, the seasonal cycle contains, at most, only 4 degrees of freedom. Thus, the statistical significance of any correlation estimated from seasonal cycles is necessarily very low.

Therefore, to statistically explore cause and effect relationships between any two time series, it is essential to first remove the seasonal cycle, thereby increasing the effective number of independent observations in the sample records. Note that this does not remove any true physical relationship between the two time series. This is because the seasonal variation of a quantity is never a pure-tone harmonic. For example, the summer maximum wind stress curl over the California Current appears earlier or later than "normal" in some years or is stronger or weaker than "normal" during some months. If a connection between the wind stress curl and a nearshore countercurrent suggested from seasonal cycles is valid, the countercurrent should similarly appear early or late, strong or weak.

Accordingly, the seasonal cycles of the wind stress curl and the steric height of the sea surface relative to 500 db were removed from the data to produce time series of nonseasonal or anomalous variability. The CalCOFI grid points used in this analysis are shown by

the dots in Figure 11 (these are the grid points occupied 40 or more times over the 30-year time period from 1950 to 1979).

The second analysis step was to extract the dominant recurring large-scale patterns of variability by computing the empirical orthogonal functions (EOFs) or principal components of nonseasonal 0/500 steric height and wind stress curl. A detailed description of this procedure and its implementation on the gappy CalCOFI hydrographic time series can be found in Chelton (1980). The principal EOF of 0/500 steric height, accounting for 31% of the overall variability, is examined in detail in Chelton (1981) and Chelton, Bernal, and McGowan (submitted). This is the mode of variability representing large-scale changes in the transport of the California Current that have been shown in the earlier studies to have an important influence on the large-scale biological variability in this region. Since it is unrelated to local wind forcing over the California Current, this pattern is not of interest to this study.

The second EOF of 0/500 steric height, accounting for 8% of the overall variability (or, equivalently, 12% of the residual variability not explained by the first EOF), is shown in Figure 11. The relatively small fraction of variability accounted for by this EOF reflects the presence of significant mesoscale energy contained in the higher order modes. This mesoscale variability is not adequately resolved (either spatially or temporally) by the CalCOFI sampling strategy, and can therefore be considered "noise" in the context of the present study. Thus, EOF analysis is a useful method for filtering this "noise" out of the data.

It can be seen from Figure 11 that this second EOF of anomalous 0/500 steric height resembles a nonseasonal analog of the seasonal California Current-Countercurrent system described earlier (with the region of flow reversal located somewhat farther offshore). The direction of geostrophic flow can be inferred from gradients of the steric height. When the time amplitude of this spatial pattern is positive, the flow in the offshore region is anomalously strong equatorward, and the nearshore flow is anomalously poleward. Correspondingly, a negative time amplitude indicates anomalous poleward flow in the region offshore, with anomalous equatorward flow nearshore. The trough (or ridge, if the sign of the time amplitude is negative) associated with these flow anomalies, shown by the dashed line in Figure 11, is located approximately 200-300 km offshore.

The time scales associated with this second EOF of nonseasonal 0/500 steric height can be determined from the autocorrelation plot in Figure 13. Typical time scales of steric height anomalies described by this pattern are around 5-6 months. This is similar to the seasonal time scales associated with an annual cycle, suggesting that this mode of variability may, indeed, represent nonseasonal (early, late, strong, or weak) variations in the seasonal countercurrent.

The hypothesis that the nearshore counterflow is forced by the wind stress curl can be examined by determining the relationship between the amplitude time series of this second EOF of anomalous 0/500 steric height and forcing by wind stress curl anomalies in this region. The most energetic aspects of large-scale wind stress curl forcing over the California Current can be described by the dominant EOF, shown in Figure 12. It is evident that the spatial resolution of these winds is very poor (the FNOC grid spacing is about 300 km at these latitudes). This coarse resolution is made even worse by the fact that the quasi-geostrophic wind stress at each grid point is determined using a differencing technique that computes pressure gradients across four grid points (a distance of about 1200 km). Then the curl of the wind stress is computed by again applying the same differencing method to the gridded wind stress values (see Caton et al. 1978 for a detailed description). Thus, the FNOC wind stress curl estimates represent only the very large-scale aspects of the wind field; spatial scales less than about 600 km are effectively filtered from the records. Even though any detailed spatial structure is obscured by this smoothing, it is still possible that the FNOC wind stress curl estimates may adequately resolve the principal time scales of the most energetic features in the wind field. The significant relation between steric height and wind stress curl demonstrated below supports this hypothesis.

In spite of the spatial smoothing, Figure 12 indicates that the first EOF of wind stress curl anomalies exhibits the general spatial characteristics desired for examining the relation between wind stress curl and anomalous nearshore countercurrents. (The correspondence between the detailed spatial structures of the steric height and wind stress curl EOFs is not as close as one would hope, but this may be due to the coarse spatial resolution of the wind data or the poor temporal resolution of the steric height data.) Wind stress curl anomalies associated with this pattern change sign some 500-600 km offshore. (Again, the sign reversal may actually occur closer to the coast, but it cannot be resolved with the coarse grid spacing of the smoothed FNOC data.) Positive time amplitudes associated with this spatial pattern correspond to anomalously high wind stress curl values nearshore. Correspondingly, negative time amplitudes refer to anomalously weak (or negative) nearshore wind stress curl. The ridge of maximum (or minimum, if the time

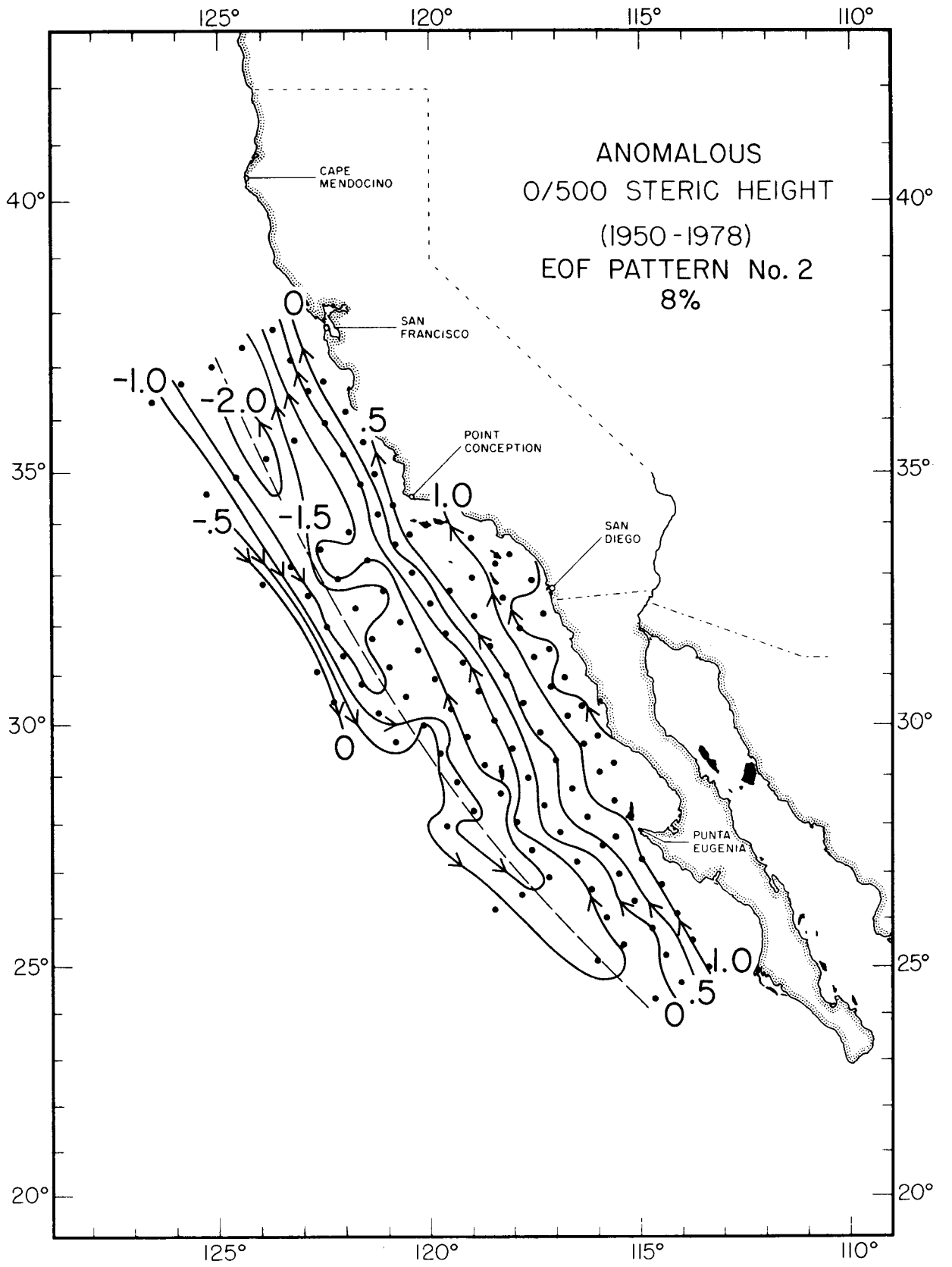

Figure 11. The second empirical orthogonal function (EOF) of nonseasonal 0/500 steric height. The seasonal means computed by the harmonic method (see Figure 4) have been removed. Dots correspond to locations of grid points over which the EOF was computed, and arrows indicate direction of geostrophic flow associated with the pattern when the time amplitude is positive.

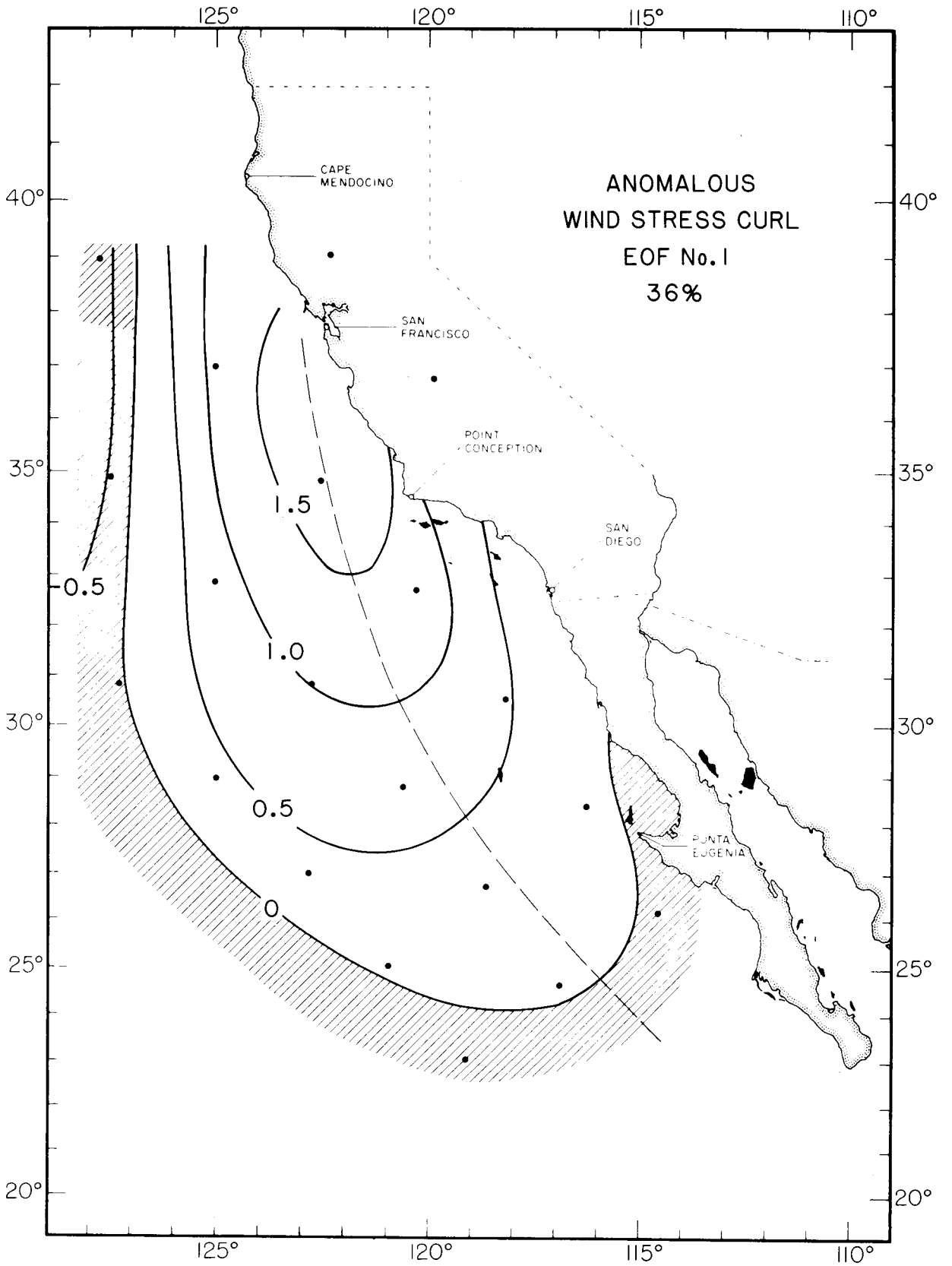

Figure 12. The first EOF of nonseasonal FNOC quasi-geostrophic wind stress curl. Again, the seasonal cycle was computed by the harmonic method and removed. Dots correspond to locations of FNOC grid points over which the EOF was computed.

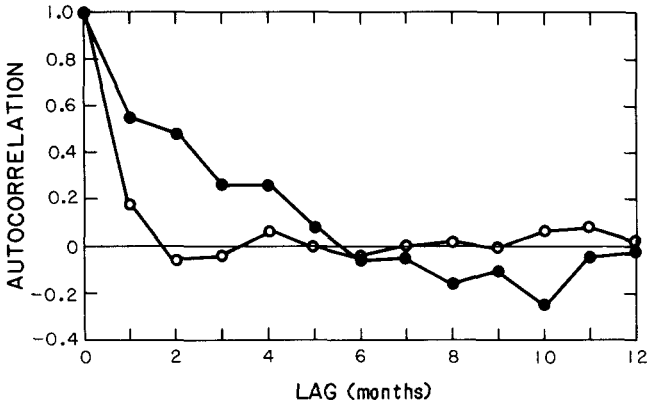

Figure 13. Autocorrelations of the amplitude time series of the second EOF of nonseasonal 0/500 steric height (solid circles) and the first EOF of nonseasonal wind stress curl (open circles).

amplitude of the pattern is negative) wind stress curl values, shown by the dashed line in Figure 12, is located 200-300 km offshore, roughly in the same location as the trough in anomalous steric height shown in Figure 11.

The time scales associated with this pattern of wind stress curl variability can be seen from Figure 13 to be very short (1-2 months). Thus, the amplitude time series of this first EOF of nonseasonal wind stress curl behaves approximately as a random, white-noise process. In view of these rapid month-to-month changes in the anomalous wind stress curl forcing, and the anticipated relatively sluggish transient adjustment of the ocean, the time-dependent Ekman pumping model (2) is likely to be a more appropriate dynamical balance than the steady-state Sverdrup balance (1).

This Ekman pumping model can be expressed in terms of centered finite differences of the amplitude time series of the steric height and wind stress curl by

$$h_2(t) - h_2(t-1) = -k \text{ curl } \vec{\tau}_1(t-\tfrac{1}{2}), \quad (3)$$

where k is a constant, h_2 refers to the amplitude time series of the second EOF of steric height, and curl $\vec{\tau}_1$ refers to the amplitude time series of the first EOF of wind stress curl. The wind stress curl data was available from FNOC in the form of 10-day averages (which were, themselves, computed from 6-hourly values of the quasi-geostrophic wind stress curl). For the analysis here, the wind stress curl at time $(t-\frac{1}{2})$ was constructed by averaging the values from the last 20 days of month $(t-1)$ and the first 20 days of month t. Thus, for example, the change of the time amplitude of the second EOF of steric height from January to February was compared with the wind stress curl averaged over the last 20 days of January and the first 20 days of February. These comparisons were made for each month when the time amplitude of the second EOF of steric height was available (a total of 90 months; see Appendix). The results were used to compute the correlation between month-to-month changes in the amplitude time series of the second EOF of steric height and the ½-month shifted-amplitude time series of the first EOF of wind stress curl. To check for the possibility of a lag in the relationship, $[h_2(t) - h_2(t-1)]$ was actually correlated with [curl $\vec{\tau}_1(t-\frac{1}{2}+T)$] for lags T ranging from -18 to 18 months. If the Ekman pumping model is valid, the only significant correlation should be at lag $T=0$.

The results are shown in Figure 14 in terms of the *skill* in estimating $\frac{dh_2}{dt}$ at time t from curl $\vec{\tau}_1$ at time $(t+T)$ (the skill is equivalent to the *squared* correlation; see, for example, Chelton, submitted[3]). The details of this skill calculation as it was applied to the gappy steric height time series are given in the Appendix. The results indicate that the only significant estimation skill indeed occurs at lag $T=0$, where the skill is 0.45 (equivalent to correlation of 0.67). This can be compared with a 95% significance skill level of 0.27 (computed as described in Chelton, submitted[3]). The positive correlation indicates that the response is as expected from the Ekman pumping model, i.e., a positive wind stress curl leads to poleward nearshore flow. This corresponds to a drop in offshore steric height and an upwelling of the thermocline offshore. (Note that the relatively large correlation at lag $T=-12$ months probably indicates the quasi-seasonality of the amplitude time series of the steric height pattern.)

This statistical result implies that, when the nearshore positive wind stress curl over the California

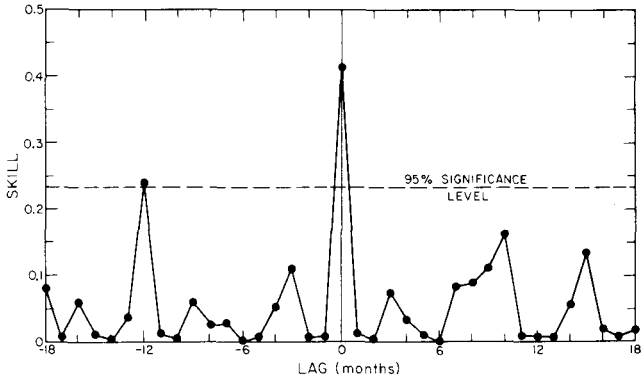

Figure 14. Skill in estimating $\frac{dh_2}{dt}$ at time t from curl $\vec{\tau}_1$ at time $(t+\text{lag})$, where h_2 refers to the amplitude time series of the second EOF of 0/500 steric height, and curl $\vec{\tau}_1$ refers to the amplitude time series of the first EOF of the wind stress curl. The quantities $\frac{dh_2}{dt}$ and curl $\vec{\tau}_1$ were approximated as centered finite differences by $|h_2(t) - h_2(t-1)|$ and curl $\vec{\tau}_1$ $(t-\frac{1}{2})$, respectively. The 95% significance level of skill values is shown by the dashed line (computed as described in Chelton, submitted. See footnote 3.) Note that skill values are equivalent to the squared correlation.

[3]Chelton, D.B. Effects of sampling errors on statistical estimation. Submitted paper.

Current is stronger than normal, the nearshore poleward counterflow is stronger than normal, and the drop in sea-surface elevation offshore (upwelling of the offshore thermocline) is greater than normal. When the nearshore positive wind stress curl is weaker than normal (or even reversed), the nearshore counterflow is correspondingly weak. In this case, the offshore sea-surface elevation is higher than normal, and the offshore thermocline is deeper than normal (upwelling is reduced).

SUMMARY AND CONCLUSIONS

The spring-summer distribution of zooplankton abundance in the California Current shown in Figures 1 and 3 reveals a somewhat surprising feature: the peak is located about 100 km offshore between San Francisco and northern Baja California. It seems unlikely that this offshore maximum is related to coastal upwelling driven by the longshore wind stress. Qualitative similarities with the seasonal nearshore counterflow and the associated offshore upwelling of the thermocline (and nutrients) suggest a possible physical-biological connection. This offshore upwelling could theoretically be forced by the unique wind stress curl conditions found to exist over the California Current. (It should be noted that similar meteorological conditions prevail over all eastern boundary currents, e.g. the Peru, Benguela, and Canary currents. Therefore, the results derived here for the California Current may be applicable to other eastern boundary currents as well.)

Although the nearshore counterflow could potentially be generated by other mechanisms (e.g., topographic steering in the Southern California Bight region), the mechanism proposed here has been demonstrated to be statistically consistent with temporal variations in the counterflow. That is, when the wind stress curl weakens, so does the nearshore counterflow. The region of offshore zooplankton maximum (San Francisco to northern Baja California) coincides with the region where the nearshore positive wind stress curl is strongest, both seasonally (see Nelson 1977; Chelton 1980) and nonseasonally (see Figure 12). To the south, where the wind stress curl is much weaker, the zooplankton maximum is located immediately adjacent to the coast.

It was emphasized that quantitative statistical examination of the relationship between the wind stress curl and the nearshore counterflow is not possible from the seasonal cycles because of the small number of degrees of freedom associated with this narrow-band process. To maximize statistical reliability, the time series must be seasonally corrected. Nonseasonal (anomalous) wind stress curl and steric height fluctuations reveal patterns analogous to their seasonal counterparts (Figures 11 and 12). These patterns can be used to statistically investigate the relationship between offshore upwelling and forcing by the wind stress curl.

From the statistical analysis of the seasonally corrected time series associated with these patterns, it is concluded that the second EOF of 0/500 steric height shown in Figure 11 resembles an Ekman pumping response to forcing by the first EOF of wind stress curl shown in Figure 12. An anomalously positive wind stress curl over the California Current generates an anomalous nearshore counterflow and upwelling of the thermocline in a region roughly parallel to the coast approximately 200-300 km offshore (coincident with the nonseasonal steric height trough in Figure 11). This large-scale upwelling is quite distinct from classical coastal upwelling, which is driven by the longshore wind stress and is limited to a region within 20-50 km of the coast. (Note that the offshore upwelling could be considered indirectly coastally related in the sense that the nearshore positive wind stress curl is "anchored" to the coast by the prevailing meteorological conditions in this region. However, the divergence of surface water responsible for the offshore upwelling is induced by horizontal shears in the long shore wind stress rather than by the discontinuity introduced by the presence of a coastal boundary.)

Although it has not been quantitatively examined in this study, it is anticipated that this Ekman pumping mechanism will prove to have important biological significance. The offshore upwelling of the thermocline provides a source of nutrients into the euphotic zone (see Figures 8 and 9) that would lead to increased productivity at all levels of the food chain. This mechanism may be responsible for the offshore peak in seasonal zooplankton abundance shown in Figures 1 and 3. In addition, the weak flow or recirculation associated with the flow reversal in the region of offshore upwelling would have little tendency to disperse the zooplankton populations, thus maintaining the high biomass. Efforts are presently under way to generate gridded time series of nonseasonal (anomalous) zooplankton biomass from the CalCOFI data. The resulting data set will allow quantitative statistical examination of the relation between the strength of the nearshore counterflow and fluctuations in zooplankton abundance.

If the hypothesis that wind stress curl-induced offshore upwelling is responsible for the offshore peak in zooplankton volume is true, then not only is coastal upwelling unimportant to the dominant large-scale variability of zooplankton abundance as demonstrated

in earlier studies by Bernal, Chelton, and McGowan, but it is also not of secondary importance (at least over the large spatial scales considered here). This would indicate that coastal upwelling effects on biological variability must be only of very localized importance (both spatially and temporally).

ACKNOWLEDGMENTS

I would like to acknowledge that the analysis described here was made possible only through the persistent and dedicated efforts of CalCOFI in collecting and archiving the 18,000 hydrocasts used to construct the 30-year time series of steric height examined in this study. Together with the 25,000 zooplankton net tows collected by CalCOFI since 1950, the CalCOFI data base is unique in its ability to study large-scale, long-term physical and biological variability. The potential for statistical examination of physical and biological interaction from this valuable data base has only begun to be exploited.

Larry Eber kindly made the CalCOFI hydrographic data available in well-organized and compacted form, and Andrew Bakun provided the FNOC wind stress curl data used in this study. John McGowan provided the station seasonal zooplankton averages from which the "pooled area" spring-summer zooplankton volumes in Figures 1 and 3 were computed. Finally, I would like to thank Joseph Reid for his continued support and encouragement during analysis of the CalCOFI data.

This work was carried out at the Jet Propulsion Laboratory, California Institute of Technology, under contract with the National Aeronautics and Space Administration.

LITERATURE CITED

Allen, J.S. 1973. Upwelling and coastal jets in a continuously stratified ocean. J. Phys. Oceanog. 3:245–257.

Bernal, P.A. 1979. Large-scale biological events in the California Current. Calif. Coop. Oceanic Fish. Invest. Rep. 20:89–101.

———. 1981. A review of the low-frequency response of the pelagic ecosystem in the California Current. Calif. Coop. Oceanic Fish. Invest. Rep. 22:49–62.

Bernal, P.A., and J.A. McGowan. 1981. Advection and upwelling in the California Current. *In* F.A. Richards, (ed.), Coastal upwelling, Amer. Geophys. Union, p. 381–399.

Caton, F.G., M.J. Cuming, and B.R. Mendenhall. 1978. A Northern Hemisphere history of marine wind-based parameters. Meteorology International, Inc., Tech. Rep. M-231, 106 p.

Chelton, D.B. 1980. Low-frequency sea level variability along the west coast of North America. Ph.D. dissertation, Scripps Institution of Oceanography, University of California, San Diego, 212 p.

———. 1981. Interannual variability of the California Current—physical factors. Calif. Coop. Oceanic Fish. Invest. Rep. 22:34–48.

———.(In press.) Statistical reliability and the seasonal cycle: comments on "Bottom pressure measurements across the Antarctic Circumpolar Current and their relation to the wind." Deep-Sea Res. Vol. 29.

Chelton, D.B., P.A. Bernal, and J.A. McGowan. (In press.) Large-scale interannual physical and biological interaction in the California Current. J. Mar. Res. 40(4).

Cushing, D.H. 1969. Upwelling and fish production. Fish. Agric. Org. Fish. Tech. Pap. 84, 40 p.

———. 1975. Marine ecology and fisheries. Cambridge Univ. Press, Cambridge, 124 p.

Davis, R.E. 1976. Predictability of sea surface temperature and sea level pressure anomalies over the North Pacific Ocean. J. Phys. Oceanog. 6:249–266.

Gill, A.E., and A.J. Clarke. 1974. Wind induced upwelling, coastal currents and sea level changes. Deep Sea Res. 21: 325–345.

Munk, W.H. 1950. On the wind-driven ocean circulation. J. Meteor. 7:79–93.

Nelson, C.S. 1977. Wind stress and wind stress curl over the California Current. NOAA Tech. Rep. NMFS-SSRF-714, August 1977.

Pedlosky, J. 1979. Geophysical fluid dynamics. Springer-Verlag, New York, 624 p.

Smith, P.E. 1971. Distributional atlas of zooplankton volume in the California Current region, 1951–1966. Calif. Coop. Oceanic Fish. Invest. Atlas 13, 144 p.

Smith, R.C., and K.S. Baker. 1982. Oceanic chlorophyll concentrations as determined by satellite (Nimbus-7 Coastal Zone Color Scanner). Mar. Biol. 66.

Smith, R.L. 1968. Upwelling. Oceanogr. Mar. Biol. Ann. Rev. 6:11–46.

Sverdrup, H. U. 1947. Wind-driven currents in a baroclinic ocean; with application to the equatorial currents of the eastern Pacific. Proc. Nat. Acad. Sci. 33:318–326.

Thomas, W.H., and D.L.R. Siebert. 1974. Distribution of nitrate, nitrite, phosphate and silicate in the California Current region, 1969. Calif. Coop. Oceanic Fish Invest. Atlas 20, 97 p.

Walsh, J.J. 1977. A biological sketchbook for an eastern boundary current. *In* The sea, Vol. 6. E.D. Goldberg, I.N. McCave, J.J. O'Brien, J.H. Steele, (eds.), Interscience, New York, p. 923–968.

Yoshida, K. 1955. Coastal upwelling off the California Coast. Recs. Oceanog. Work Jap. 2: 8–20.

Yoshida, K., and H. Mao. 1957. A theory of upwelling of large horizontal extent. J. Mar. Res. 16:134–148.

APPENDIX

Computation of the correlation between time derivatives of the steric height and the wind stress curl is hindered by the fact that the steric height time series is gappy. This gappiness in both space and time required special techniques for generating the amplitude time series of the empirical orthogonal functions (EOFs). Computation of the time amplitude for a given month requires data values for that month at each of the N grid points used to generate the EOF. Since there were no months when all 150 of the grid points shown in Figure 11 were occupied, a technique for objectively estimating the EOF time amplitudes from the existing data values was required. The method developed by Davis (1976) was used, and the details are described in Chelton (1980). Objectively estimated time amplitudes for months with expected square errors exceeding 30% of the variance associated with the EOF were rejected, so that the time amplitudes for those months were considered "missing." For the time amplitudes of the second EOF of 0/500 steric height, this objective estimation scheme produced 90 months of "acceptable" data.

For ease of notation, define

$$H(t) = h_2(t) - h_2(t-1)$$
$$X(t) = \text{curl } \vec{\tau}_1(t-\tfrac{1}{2}),$$

where h_2 is the amplitude time series of the second EOF of steric height, and curl $\vec{\tau}_1$ is the amplitude time series of the first EOF of wind stress curl. Then the centered difference Ekman pumping model (3) reduces to

$$H(t) = -k\,X(t). \tag{4}$$

The most obvious method of examining this model statistically is to compute the time series $H(t)$ and $X(t)$ and simply correlate them. Using $< >$ to denote the expected or mean value, this correlation is given by

$$R_{HX} = \frac{<H(t)\,X(t)>}{[<H^2(t)><X^2(t)>]^{1/2}} \tag{5}$$

However, although the number of sample values of $h_2(t)$ was 90, there were only 40 months t when both $h_2(t)$ and $h_2(t-1)$ existed, i.e. 40 values of $H(t)$. Then the correlation computed by (5) would be based on only 40 data values resulting in very low statistical reliability of the correlation estimate.

Therefore, an alternative method was developed; it involves computing the *statistics* of $H(t)$ rather than $H(t)$ itself. To see how this is done, substitute $[h_2(t) - h_2(t-1)]$ for $H(t)$ in (5) to get

$$R_{HX} = \frac{<h_2(t)\,X(t)> - <h_2(t-1)\,X(t)>}{2^{1/2}[(<h_2^2(t)> - <h_2(t)\,h_2(t-1)>)<X^2(t)>]^{1/2}} \tag{6}$$

In this last expression, the steric height EOF time series $h_2(t)$ has been assumed to be stationary. Since the wind stress curl time series $X(t)$ is complete, and only $h_2(t)$ is gappy, with the exception of the term $<h_2(t)\,h_2\,(t-1)>$, all of the statistical quantities in (6) can be estimated from all 90 months t when $h_2(t)$ exists: $<h_2(t)\,h_2(t-1)>$ must be estimated from only the 40 months when both $h_2(t)$ and $h_2(t-1)$ exist. Consequently, the statistical reliability of this quantity is lower than that of the others. However, since $<h_2(t)\,h_2(t-1)>$ is only about half as large as $<h_2^2(t)>$ (see Figure 13), the sensitivity of (6) to errors in this term is relatively small. Thus, use of (6) to compute the correlation between $H(t)$ and $X(t)$ is more reliable than first computing $H(t)$ and correlating the resulting time series with $X(t)$ as in (5).

In computing the correlation between $H(t)$ and $X(t)$, the model (4) was generalized to allow for the possibility of a lagged relationship:

$$H(t) = -k\,X(t+T)$$

where $X(t+T) = \text{curl } \vec{\tau}_1(t-\tfrac{1}{2}+T)$. The skill in estimating $H(T)$ from $X(t+T)$ is equal to the square of the correlation as computed by (6) [with $X(t)$ replaced by $X(t+T)$]. These skill values are plotted in Figure 14 for lags T ranging from -18 to 18 months.